PHIL Test Bench for Online-Identification Methods of Complex Power Grid

T. Reinikka * **R. Luhtala** * **H. Alenius** ** **T. Roinila** *
T. Messo **

* *Automation and Hydraulic Engineering, Tampere University of Technology,Tampere, Finland (e-mail: tommi.reinikka@tut.fi).*
** *Electrical Energy Engineering, Tampere University of Technology,Tampere, Finland (e-mail: tuomas.messo@tut.fi)*

Abstract:
Power generation is shifting towards renewable and distributed energy production due to increased awareness of climate change and the recent advancements in renewable technologies. Distributed energy generation typically consists of wind and solar power plants, virtually all of which are connected to power grid by an inverter. As a consequence, the stability issues generated by the active power electronic devices are continuously increasing. The increased requirements for the functionality of the grid-connected inverters require a sophisticated test bench for experimentation. Power hardware-in-the-loop methods allow combining of the simulations to actual hardware, and thus, enable running experiments on real devices in time-varying conditions. This paper presents the use of a power hardware-in-the-loop test bench for stability studies of grid-connected systems. Experimental MIMO measurements based on pseudo-random sequences injected with a three-phase grid-connected inverter are presented and used to demonstrate the effectiveness of the proposed method.

Keywords: Electric power systems, MIMO, Power hardware-in-the-loop, Pseudo-random sequences, Real-time identifications

1. INTRODUCTION

Concern about climate change and the decreased costs of renewable production have shifted the focus of power production towards environmentally sustainable alternatives (Bose (2013)). These consist mainly of wind and solar power which are most commonly connected to the grid through a power electronic inverter. Traditional large synchronous generators are being replaced by inverters which are more prone to stability issues. Stability issues have been already reported in locations with a high share of power generated through inverters (Li (2017)).

Power electronics have a major impact on the dynamics of the power grid. The interaction issues between the inverters and power grid have been researched extensively (Luhtala et al. (2017), Shi et al. (2017)). The capability to provide voltage support and fault ride-through are already required from the inverters and frequency support is required for renewable energy source connected to certain power grids (Brisebois and Aubut (2011)). As the grid conditions significantly vary over time, the stability of the inverters must be guaranteed in a wide range of scenarios.

The dynamics of a grid-connected system can be efficiently studied through the impedance-based stability criterion (Messo et al. (2015)) in which the inverter and grid impedances are studied and analyzed. Mismatching these impedances could cause harmonic resonances or even instability (Sun (2011)). Therefore, the grid impedance is an important factor when assessing the stability of grid-connected devices. Traditionally, grid impedance has been modeled with simplified constant resistance and inductance. However, as the grid conditions vary over time, the models that apply constant variables are often inaccurate (Jessen and Fuchs (2015)).

In the analysis of time-variant dynamics of grid-connected systems, real-time identification methods are most desirable. Recent studies have shown several applications for such identification approach (Messo et al. (2017), Timbus et al. (2006), Cespedes and Sun (2012)). These studies have presented efficient online techniques, but only very simple power grids have been considered. As the practical structure of the power grid may be very complex, there is a strong need for a test bench in which the power grid can be realistically considered.

The present paper introduces a test bench for real-time identification of a complex power grid. A power hardware-in-the-loop (PHIL) implementation is presented using a photovoltaic inverter and emulated grid impedance. The PHIL method enables the connection of a real inverter to complex grid models, and thereby providing a versatile tool for stability assessment in realistic grid conditions. This allows the experiments to be carried out on real devices instead of pure software environment.

The remainder of this paper is organized as follows. Section 2 reviews the stability analysis of grid-connected devices and grid impedance modeling technique. Section 3 introduces the PHIL method and reviews the utiliza-

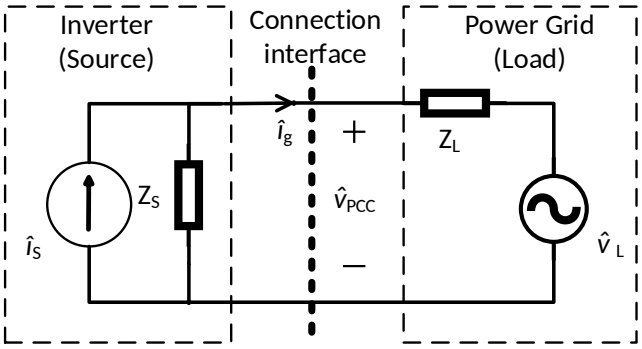

Fig. 1. Equivalent circuit of inverter-grid connection.

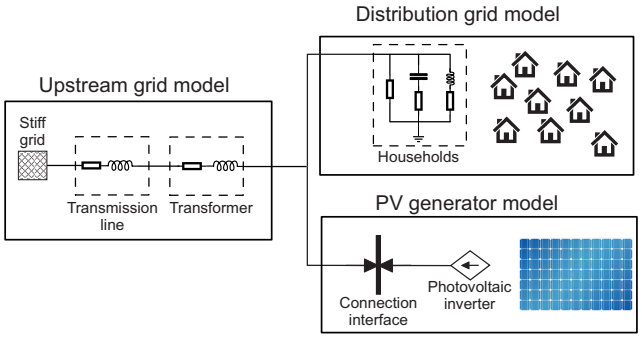

Fig. 2. Power grid topology using sub-models.

tion of uncorrelated signals for multiple-input-multiple-output (MIMO) identification tool for measuring the grid impedance in real-time. Section 4 shows a practical implementation for PHIL test bench. Experimental results are shown in Section 5, and Section 6 draws conclusions.

2. THEORY

2.1 Impedance-based stability analysis

Fig. 1 shows the equivalent circuit for inverter-grid connection. The inverter is modeled as an ideal current source with a parallel impedance and the grid is modeled as an ideal voltage sink with series impedance. The grid and inverter are assumed to be stable when operated independently from each other. The grid current can be derived as (Sun (2011))

$$\hat{i}_g(s) = \left(\hat{i}_{inv}(s) - \frac{\hat{v}_g(s)}{Z_{inv}(s)}\right)\left(\frac{1}{1 + Z_g(s)/Z_{inv}(s)}\right).$$

where $\hat{i}_{inv}(s)$ is current of the ideal source, $Z_{inv}(s)$ models finite output impedance of the inverter, $\hat{v}_g(s)$ is the ideal voltage sink (stiff grid), and $Z_g(s)$ describes non-ideality of the grid side. Because of the assumptions that the inverter and the grid themselves are stable, the stability of the grid current can be studied by the transfer function

$$G(s) = \frac{1}{1 + Z_g(s)/Z_{inv}(s)} \tag{1}$$

The transfer function resembles a basic closed-loop transfer function of a negative feedback system, so the conventional Nyquist stability criterion applies. Hence, the system is stable if the impedance ratio $Z_g(s)/Z_{inv}(s)$ satisfies the Nyquist stability criterion.

2.2 Complex grid impedance

The impedance of a power grid is a transfer function from current to voltage, and always relates to certain point of common coupling (PCC). It consists of interconnected impedances of grid elements, generators, and loads. The layout of the power grid can significantly vary depending on the location of the PCC. In this paper, the grid impedance is analyzed based on sub-models. Fig. 2 shows the topology of the power grid and the interface in which the stability assessment is applied. The high-voltage upstream grid is usually mainly inductive due to inductive transmission lines and transformers (Jessen et al. (2015)). However, in a low-voltage distribution grid

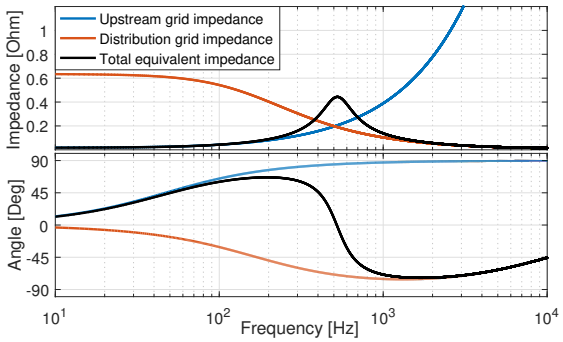

Fig. 3. Formation of equivalent grid impedance.

the stray capacitances and capacitive loads may add up to significant equivalent capacitance, as the equivalent parallel capacitance is given from $C_{eq} = \Sigma C$. On the other hand, the impact of parallel-connected inductors diminishes based on $L_{eq} = 1/\Sigma(L^{-1})$.

Parallel-connected inductive and capacitive sub-models form the equivalent grid impedance, as shown in Fig. 3. Consequently, a parallel LC-resonance appears as a peak in magnitude. The equivalent impedance for un-damped parallel resonance is given by

$$Z_{eq} = \frac{1}{(j2\pi f L_{eq})^{-1} + j2\pi f C_{eq}} \tag{2}$$

where the denominator approaches zero at the resonant frequency $f_{res} = 1/(2\pi\sqrt{LC})$. This resonant frequency can be as low as 250 Hz (Enslin and Heskes (2004)).

2.3 Time variance of grid impedance

The active power consumed in a real power grid defines the equivalent resistance. Thus, a real grid impedance contains resistive element in addition to resonant L and C elements. This resistance effectively damps the LC-resonance. However, as the loads are time variant, the damping varies accordingly. (Knop and Fuchs (2009). Fig. 4 presents an LC resonant circuit with different damping resistances. A higher active power corresponds to lower equivalent parallel resistance, which increases damping and, consequently, the resonance peak is lower. Especially high resonant peaks occur when the active power consumption is very low.

The inductance of the upstream subsystem remains almost constant, but the capacitance in the distribution subsys-

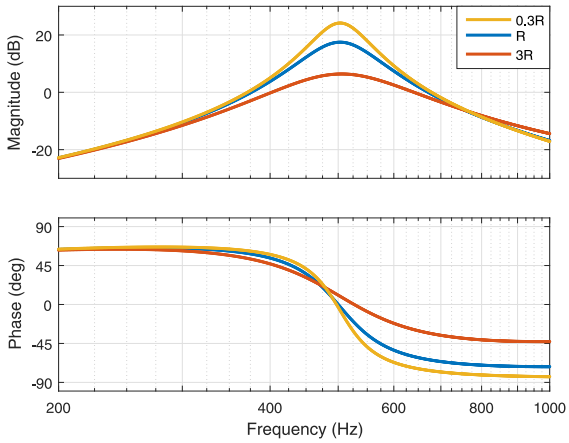

Fig. 4. Simplified grid impedance with varying loadings.

tem may vary. Therefore, the resonant frequency changes as the total equivalent capacitance varies.

3. METHODS

3.1 Power hardware-in-the-loop implementation

The grid impedance is affected by the layout of the power grid connected to the PCC and the power flows of the grid. In this work, the response of the grid to the connected device is simulated with a real-time digital power system -simulator (RTDS). This allows the power grid to be modified online; for example, by tripping parts of the grid or changing the power flows of the power grid.

The downside of the emulated power grid is that the simulated response causes delay to the system. This delay, combined with the A/D conversion between the simulator and the hardware, means that there is always some error in the emulated voltage (Ren et al. (2008)). The error may cause the system to lose stability even if the emulated system would be normally stable (Hong et al. (2009)). The stability of the PHIL-power grid emulation must be guaranteed before turning the system on.

The stability of the grid emulation in PHIL system can be assessed by knowing the transfer functions of the used equipment and the interface algorithm used for connecting the hardware to the simulation. Fig. 5 illustrates the interface algorithm used in this system. The method is also known as an ideal transformer method. Current measurements from the hardware side are connected to the simulation as current sources and voltage values of the connection point are used as the voltage reference for the grid emulator. The transfer function of the power grid can be represented as (Lehfuss and Lauss (2011))

$$G_{grid} = e^{-s\Delta T_\mathrm{d}} \frac{Z_\mathrm{s}}{Z_\mathrm{HW}} T_\mathrm{amp} T_\mathrm{filt} \tag{3}$$

where $e^{-s\Delta T_\mathrm{d}}$ is an approximation of the effect of the delay in the grid emulation, Z_s is the simulated impedance, Z_HW is the hardware impedance, T_amp is the voltage amplifier transfer function, and T_filt is the low-pass filter transfer

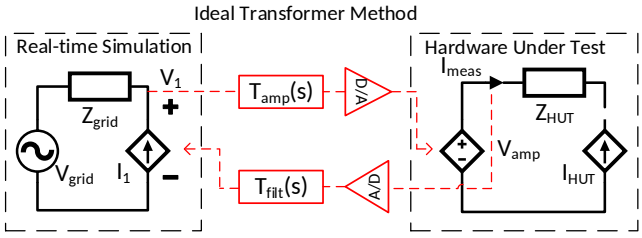

Fig. 5. Ideal transformer method interface algorithm

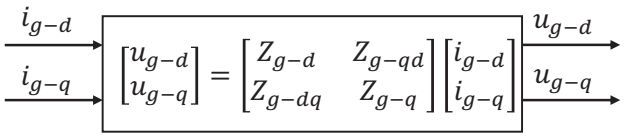

Fig. 6. Representation of dq-domain impedances.

function. The transfer function of the interface must fulfill the Nyquist stability criterion for stable operation.

3.2 Orthogonal pseudo-random sequences

The grid-connected systems are often modeled in the synchronous reference frame (dq domain), where three-phase waveforms are transformed (in synchronous case) to two DC-valued components, direct (d) and quadrature (q). The transformation to dq domain introduces cross-couplings between the components; the fully characterized system includes individual impedances for both components and cross-coupling impedances between the components. Fig. 6 illustrates the multiple-input-multiple-output (MIMO) nature of the impedance in the dq-domain. The cross-coupling impedances are usually small enough to be neglected (Wen et al. (2017)); however, when reactance of the system increases, the cross-couplings must be taken into account in order to avoid inaccuracy.

In MIMO systems, all the input and output couples can be measured one by one. However, this approach may be time-consuming and the operating conditions can change between measurement cycles. However, it is possible to measure all transfer functions of MIMO system simultaneously by using signals that have energy at different frequencies. This kind of signals are known as uncorrelated signals. By using two uncorrelated signals to perturb both components, the individual and cross-coupling impedances of d and q components can be measured simultaneously.

Godfrey (1993) has introduced uncorrelated signals that have the characteristics of well-known maximum-length binary sequences (MLBS). These signals have been shown to be effective in online measurements in numerous applications (Luhtala et al. (2018), Roinila et al. (2013), Roinila et al. (2014)). The MLBS fits the purpose of the paper as the signal can be averaged over many periods. The noise in the system varies due to the power grid layout changing over time. The technique of producing two MLBS-based uncorrelated signals starts by generating a conventional MLBS. The orthogonal sequence is obtained by first doubling the MLBS and then inverting every other digit of the doubled sequence. The second sequence is known as inverse-repeated sequence (IRS). Fig. 7 shows the power

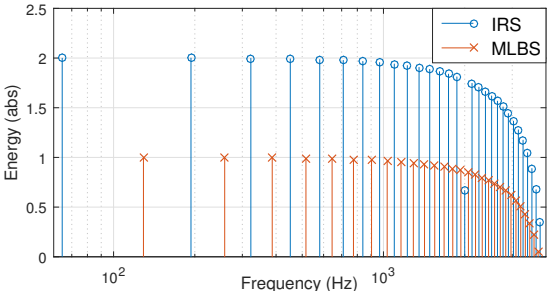

Fig. 7. Power spectrum of 31-bit-length MLBS and corresponding IRS generated at 4 kHz.

spectra of 31-bit-length MLBS and corresponding IRS. The values are scaled to facilitate the illustration.

4. IMPLEMENTATION

4.1 Test bench

Fig. 8 shows the layout of the laboratory setup. The PV-emulator feeds the input power to the inverter, which is connected to a three-phase linear voltage amplifier. The inverter is controlled using a dSPACE real-time simulator, PV-emulator follows a predetermined I/V-curve and the grid emulator is connected to a real-time digital simulator (RTDS). Current measurements from the hardware are fed as inputs to RTDS, which generates the voltage references for the grid emulator.

The grid emulation is performed on the RTDS with a sampling frequency of 40 kHz. The total delay in the system is 136.6μs. The delay is caused by the simulation step size, A/D and D/A conversion and the voltage amplifier. For stable operation the current measurements fed to the grid simulation must be lowpass-filtered. The cutoff frequency of the filter is set to 10.5 kHz. The setup allows emulating the grid frequency response accurately up to range of 1 kHz (Reinikka et al. (2018)).

4.2 Real-time identifications

When measuring the grid impedance, the perturbations must be injected from the inverter side. The applied implementation in this paper does not require any external signal generators because the inverter itself generates the perturbation signals to its output currents. In the implementation, the MLBS is added to a current reference of d component and the IRS to q component of the inverter current controllers. The q-channel has inherently lower power, and thus the IRS is better choice to be applied to q component.

As Fig. 8 shows, the interconnection point is considered so that the second inductor of LCL- type filter and the isolation transformer are included to the grid-impedance. Hence, v_o and i_o are continuously captured and transformed to the dq domain. The grid impedance is computed as a ratio of Fourier transformed voltage and current using cross-correlation techniques (Godfrey (1993)). MATLAB/Data Acquisition Toolbox is configured to operate the measurement card and compute the grid-impedance in real-time.

5. EXPERIMENTS

5.1 Experimental setup

In the experiments, the equivalent grid impedance is modeled as a parallel connection of the inductive upstream grid and the distribution grid. The distribution grid is considered to consist of a group of households. According to Enslin and Heskes (2004), a typical household has equivalent capacitance of between 0.6 ... 6 μF and the equivalent resistance varies with the actual power consumption.

Table 1 shows the parameters for three experimental grids. Case 1 models realistic connection point for the photovoltaic inverter at the night time: distribution grid includes 50 households with an average of 5 μF capacitance and low power consumption (high resistance). Cases 2 and 3 present very weak grid conditions in two different loading scenarios. There are more capacitive loads at the distribution-grid side and relatively long low-voltage transmission line before the transformer at the upstream-grid side which introduces higher inductance.

Table 1. Experimental grids

	R_{load}	C_{eq}	L_{grid}
Case 1	10 Ω	250 μF	180 μH
Case 2	8 Ω	400 μF	400 μH
Case 3	3 Ω	400 μF	400 μH

The MIMO measurements in the experiments are performed using a 2047-bit-long MLBS and corresponding IRS, both generated at 4 kHz. This provides impedance measurements with a frequency resolution of 1.95 Hz and measurement time of 0.51 s for one cycle. Online measurements demand very low injection amplitude, so that the produced power quality is not affected too much. The amplitudes are set to be less than 0.2 percent of the nominal inverter output current. Due to very low injection amplitude, more averaging is required in order to get accurate measurements. The results are averaged over 116 periods, which means the refresh rate of the results is approximately one minute. In these experiments, the accuracy and low amplitude of the injections are more desirable than short measuring time. However, the measurement setup is very flexible and can be configured, for example, to provide very fast measurements by readjusting the parameters.

5.2 Real-time MIMO measurements

Figs. 9 and 10 show the impedance measurements obtained by real-time MIMO methods and compared to results obtained by a commercial frequency response analyzer, which is based measuring the d and q components separately with sinesweep method. Case 1 shown in Table 1 and in Fig. 8 is used as the emulated grid. Case 1 has parallel and series resonance at 750 Hz.

The measurements performed with the MLBS are accurately following the curves measured with the frequency response analyzer in both magnitude and phase. The measured impedance is strongly affected by the LCL-filter and isolation transformer but the dq-domain measurements show emulated resonant peak at the predicted value. The

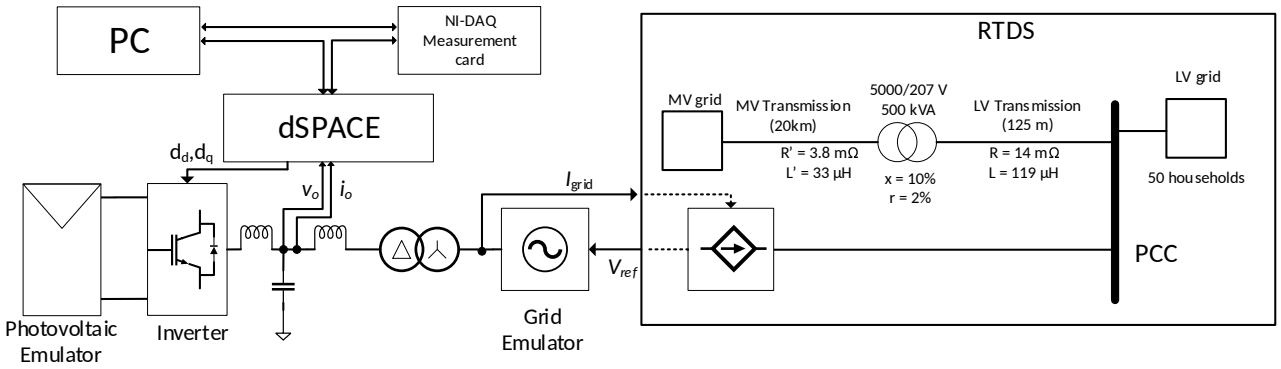

Fig. 8. Layout of the test bench and the emulated power grid

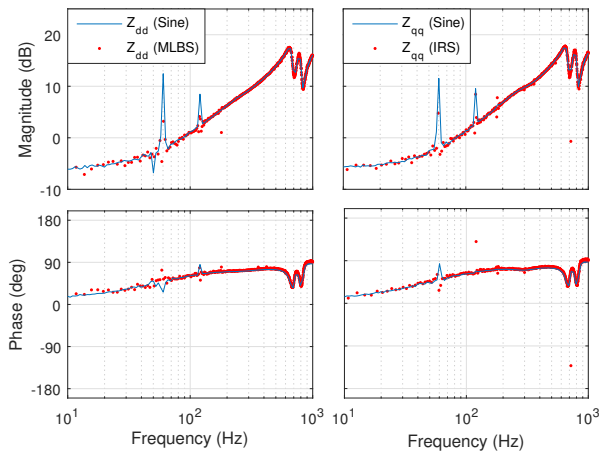

Fig. 9. Grid-impedance measurements of d and q-components.

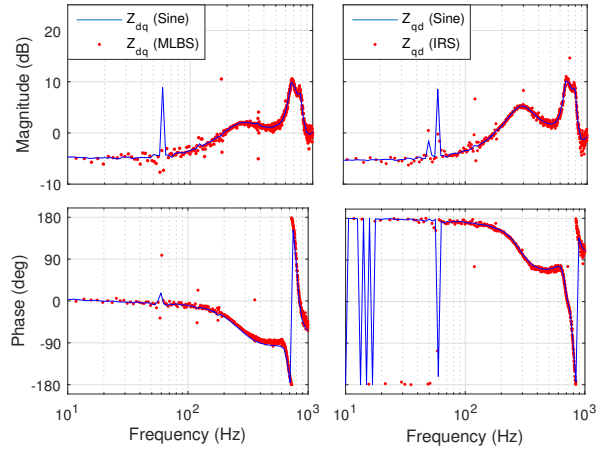

Fig. 10. Grid-impedance measurements of dq and qd crosscouplings

parallel resonance is seen in dq-domain as two peaks instead of one due to rotating frame in dq-transformation. The first peak is located one fundamental frequency below the phase-domain peak and the second peak is located one fundamental frequency above the phase-domain peak. The peak at 60 Hz is caused by measurement noise at fundamental frequency and as such can be ignored.

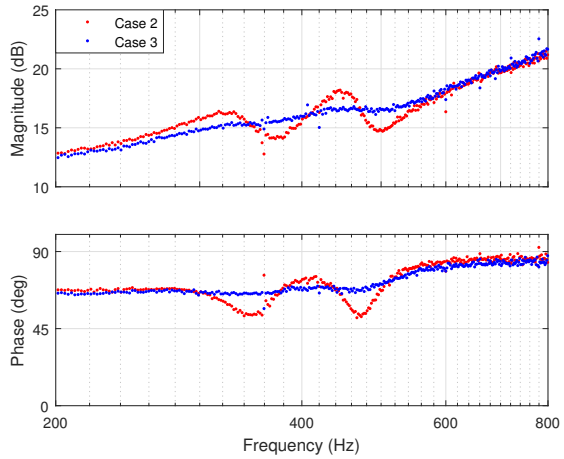

Fig. 11. Grid-impedance d-component measurement in low (Case 2) and high (Case 3) power flow scenarios

5.3 Load scenarios

Fig. 11 shows measurements of two different grid impedance emulations. The scenario represents the grid-impedance measurement from the same grid-connection point at day and night. In such a situation, the active power consumption at the distribution grid varies and corresponds to different resistive loads. Case 2 includes less active power consumption which results in a clear resonance peak at 450 Hz. Active power consumption is increased in Case 3 and the resonance peak is damped, due to lower equivalent resistance of the higher power consumption.

These experiments have clearly shown that the grid impedance varies over time with multiple parameters and that modeling the impedance only as a series resistance and inductance is insufficient in many cases. LC-resonance, caused by inductive upstream grid and capacitive distribution grid, may cause issues in the impedance-based stability assessment. These resonances should be taken into account in order to ensure system stability.

6. CONCLUSION

The impedance-based stability issues of grid-connected systems have emerged as a problem as the amount of renewable energy production has increased. The time-varying grid impedance has been shown to have a major effect on system dynamics and stability. There has been a

lack of inverter experimentation with complex grid models, and the grid is often modeled as a mere inductor. The emulated power grid in power hardware-in-the-loop test bench makes it possible to run tests in time-varying grid conditions and provides a powerful tool for recreating and studying the issues reported in grid-connected power electronics.

This paper has shown an implementation of a test bench where the dynamics of grid-connected systems can be analyzed under time-varying, realistic test conditions. The presented methods can be used for detailed stability analysis and adaptive control implementations of grid-connected systems.

REFERENCES

Bose, B.K. (2013). Global energy scenario and impact of power electronics in 21st century. *IEEE Transactions on Industrial Electronics*, 60(7), 2638–2651.

Brisebois, J. and Aubut, N. (2011). Wind farm inertia emulation to fulfill hydro-quebec's specific need. In *2011 IEEE Power and Energy Society General Meeting*, 1–7.

Cespedes, M. and Sun, J. (2012). Online grid impedance identification for adaptive control of grid-connected inverters. In *2012 IEEE Energy Conversion Congress and Exposition (ECCE)*, 914–921.

Enslin, J.H.R. and Heskes, P.J.M. (2004). Harmonic interaction between a large number of distributed power inverters and the distribution network. *IEEE Transactions on Power Electronics*, 19(6), 1586–1593.

Godfrey, K.R. (1993). *Perturbation Signals for System Identification*. Prentice Hall, UK.

Hong, M., Horie, S., Miura, Y., Ise, T., and Dufour, C. (2009). A method to stabilize a power hardware-in-the-loop simulation of inductor coupled system.

Jessen, L. and Fuchs, F.W. (2015). Modeling of inverter output impedance for stability analysis in combination with measured grid impedances. In *2015 IEEE 6th International Symposium on Power Electronics for Distributed Generation Systems (PEDG)*, 1–7.

Jessen, L., Gunter, S., Fuchs, F.W., Gottschalk, M., and Hinrichs, H.J. (2015). Measurement results and performance analysis of the grid impedance in different low voltage grids for a wide frequency band to support grid integration of renewables. In *2015 IEEE Energy Conversion Congress and Exposition (ECCE)*, 1960–1967. ID: 1.

Knop, A. and Fuchs, F.W. (2009). High frequency grid impedance analysis by current injection. In *2009 35th Annual Conference of IEEE Industrial Electronics*, 536–541. ID: 1.

Lehfuss, F. and Lauss, G. (2011). Power hardware-in-the-loop simulations for distributed generation. In *21st International Conference on Electricity Distribution*, 1–4.

Li, C. (2017). Unstable operation of photovoltaic inverter from field experiences. *IEEE Transactions on Power Delivery*, (99), 1–1.

Luhtala, R., Messo, T., Roinila, T., Reinikka, T., Sihvo, J., and Vilkko, M. (2017). Adaptive control of grid-connected inverters based on real-time measurements of grid impedance: Dq-domain approach. In *2017 IEEE Energy Conversion Congress and Exposition (ECCE)*, 69–75.

Luhtala, R., Roinila, T., and Messo, T. (2018). Implementation of real-time impedance-based stability assessment of grid-connected systems using mimo-identification techniques. *IEEE Transactions on Industry Applications*.

Messo, T., Aapro, A., and Suntio, T. (2015). Generalized multivariable small-signal model of three-phase grid-connected inverter in dq-domain. In *2015 IEEE 16th Workshop on Control and Modeling for Power Electronics (COMPEL)*, 1–8.

Messo, T., Luhtala, R., Roinila, R., Yang, D., Wang, X., and Blaabjerg, F. (2017). Real-time impedance-based stability assessment of grid converter interactions. In *the Eighteenth IEEE Workshop on Control and Modeling for Power Electronics, IEEE COMPEL 2017*.

Reinikka, T., Alenius, H., Roinila, T., and Messo, T. (2018). Power hardware-in-the-loop setup for stability studies of grid-connected power converters. In *The 2018 International Power Electronics Conference, IPEC -ECCE Asia*.

Ren, W., Steurer, M., and Baldwin, T.L. (2008). Improve the stability and the accuracy of power hardware-in-the-loop simulation by selecting appropriate interface algorithms. *IEEE Transactions on Industry Applications*, 44(4), 1286–1294.

Roinila, T., Vilkko, M., and Sun, J. (2013). Broadband methods for online grid impedance measurement. In *2013 IEEE Energy Conversion Congress and Exposition*, 3003–3010.

Roinila, T., Vilkko, M., and Sun, J. (2014). Online grid impedance measurement using discrete-interval binary sequence injection. *IEEE Journal of Emerging Selected Topics In Power Electronics*, 2(4), 985–993.

Shi, Y., Wang, L., and Li, H. (2017). Stability analysis and grid disturbance rejection for a 60kw sic based filterless grid-connected pv inverter. *IEEE Transactions on Industry Applications*, PP(99), 1–1.

Sun, J. (2011). Impedance-based stability criterion for grid-connected inverters. *IEEE Transactions on Power Electronics*, 26(11), 3075–3078.

Timbus, A.V., Teodorescu, R., Blaabjerg, F., and Borup, U. (2006). Online grid impedance measurement suitable for multiple pv inverters running in parallel. In *Twenty-First Annual IEEE Applied Power Electronics Conference and Exposition, 2006. APEC '06.*

Wen, B., Burgos, R., Boroyevich, D., Mattavelli, P., and Shen, Z. (2017). Ac stability analysis and dq frame impedance specifications in power-electronics-based distributed power systems. *IEEE Journal of Emerging and Selected Topics in Power Electronics*, 5(4), 1455–1465.